


Handbook
for
Generic Photonic IC Design

Editors: Meint Smit and Xaveer Leijtens

4-4-2026

 *Handbook for generic photonic IC design*, by the *Photonic Integration group*, Technische Universiteit Eindhoven, is licensed under a Creative Commons “Attribution-NonCommercial-NoDerivatives 4.0 International” license.

We traced the ownership of all figures used as far as we could. However, if you are a copyright owner and believe we used your work without permission, please contact us at coordinator@jeppix.eu.

Chapter 19

Multi-Mode Interference Devices

XAVEER LEIJTENS AND MEINT SMIT

19.1 Introduction

Waveguide couplers can be used for coupling light between two or more waveguides, for splitting power from one to a number of waveguides (power splitter) or combining light from a number of waveguides into a single waveguide (power combiner). Figure 19.1 shows a number of different couplers. Couplers a), b) and c) are $1 \times N$ couplers. Couplers d), e) and f) are $M \times N$ couplers, they couple light from multiple input ports to multiple output ports. *waveguide coupler*
power splitter
power combiner

We can distinguish between different types of couplers: branching (Y-junctions), radiation couplers, evanescent wave couplers, and couplers based on self-imaging. The latter are usually called Multi-Mode Interference (MMI) devices. They are used most frequently in high-contrast waveguide systems, like in semiconductor-based PICs. They have the advantage that they are compact, but at their interfaces with the input and output waveguides they experience loss and reflections. By proper design the loss can be minimized below a few tenths of a dB and the reflection below -30 dB. *MMI*

MMI-devices are composite building blocks: they consist of a multi-mode waveguide section and two junctions with other waveguides at both sides of the multi-mode waveguide. In this chapter we describe the MMI-couplers and a few other devices which are based on Multi-Mode Interference, such as filters and reflectors. The other couplers are described in following chapters.

19.2 Multi-Mode Interference (MMI) and Self-Imaging

Figure 19.2 shows a simulated intensity pattern in a multi-mode waveguide section and the corresponding experimentally imaged pattern. At the left side light is coupled into the device from a narrow single-mode waveguide. In the wide section the light is no longer laterally confined and starts to diffract into a divergent beam. After propagating some distance it is reflected by the side walls and starts interfering with itself, which gives rise to a fascinating interference pattern. At the right hand side of the wide waveguide section all the light focuses in two spots: a double image of the input beam. At two thirds of the imaged length the input beam appears to image in three spots.

Halfway we observe four images and a bit before that five and even six images. The experimentally imaged pattern shows how good the experimental results agree with the simulation.¹

If we connect two output waveguides at the end, as shown in figure 19.2d, we have a 1×2 power splitter. If we cut the waveguide at half of its length, as shown in figure 19.2c, and connect four output waveguides, we have a 1×4 splitter.

self-imaging In the following paragraphs we will give an explanation of the self-imaging properties of multi-mode waveguides and discuss a number of applications.

19.3 Analysis of the imaging mechanism

imaging To analyze the imaging properties of a multi-mode waveguide section we decompose the exciting field $U(y,0)$ at the input junction of the waveguide into its modal components, propagate them through the waveguide and reconstruct the field at the end of the waveguide as the sum of the modes.

The lateral field $U(y,0)$ at the input can be described as:

$$U(y,0) = \sum a_m U_m(y) \quad (19.1)$$

in which $U_m(y)$ is the field of mode m and a_m is its excitation coefficient. The complex modal excitation coefficients a_m of each of the modes U_m in the multi-mode waveguide section, by the input field $U(y,0)$ can be calculated with the overlap integral:

$$a_m = \frac{\int U(y,0) U_m(y) dy}{\sqrt{\int |U(y,0)|^2 dy \cdot \int |U_m(y)|^2 dy}} \quad (19.2)$$

The field $U(y,L)$ at length L follows as:

$$U(y,L) = \sum a_m U_m(y) \cdot e^{-j\beta_m L} \quad (19.3)$$

in which β_m is the propagation constant of mode m . The shape of $U(y,L)$ is only dependent on the phase difference between the modes, so we can take the phase factor $e^{-j\beta_0 L}$ of the fundamental mode out of the summation. We then find

$$U(y,L) = \sum a_m U_m(y) \cdot e^{-j(\beta_m - \beta_0)L} = \sum a_m U_m(y) \cdot e^{j\Delta\beta_{0m}L} \quad (19.4)$$

in which

$$\Delta\beta_{0m} = \beta_0 - \beta_m \quad (19.5)$$

If the phase difference $\Delta\beta_{0m}L$ of all the modes with the fundamental mode equals a multiple of 2π , then the field at that length will be an image of the input field, which explains the name self-imaging which is sometimes used for Multi-Mode Interference.

Multi-Mode Interference The lengths at which this self-imaging occurs can be found by analyzing the relation between the longitudinal and the lateral propagation constants. Figure 19.3 illustrates

¹The experimental image has been measured in an Al_2O_3 waveguide, which was heavily doped with Erbium atoms [278]. In such a highly doped waveguide coupled Erbium atoms can absorb the energy of a number of infrared photons (1550 nm) and emit it as green light (upconversion). The green light is emitted in all directions and it is proportional to (the fourth power of) the IR-intensity. By making a photograph of the green light pattern as seen through a microscope above the wafer we get an image of the IR intensity pattern in the waveguide, but imaged with green light. Because the wavelength of green light is three times shorter than the IR wavelength, we can image the IR light pattern with a resolution far below the diffraction limit of IR-light. A simple microscope is, therefore, sufficient to make a high-resolution image of the IR intensity pattern as shown in Figure 19.2.

their dependence. In strongly multi-moded waveguides the lower order modes will be almost completely confined so that their lateral mode profiles will contain an integer number of half periods within the waveguide. Therefore, the higher-order mode profiles are spatial harmonics of the fundamental mode profile and their lateral propagation constants k_{ym} will be integer multiples of the fundamental one (see Chapter 2, Sec. 2.2.2):

$$\begin{aligned} k_{ym} &\simeq (m+1)k_{y0} \\ k_{y0} &\simeq \pi/W \end{aligned} \quad (19.6)$$

lateral propagation constant

in which m is the number of the mode and W is the width of the multi-mode waveguide section. The corresponding propagation constant β_m follows as:

$$\beta_m = \sqrt{N_{\text{core}}^2 k_0^2 - k_{ym}^2} \approx N_{\text{core}} k_0 - \frac{1}{2} (m+1)^2 \frac{k_{y0}^2}{N_{\text{core}} k_0} \quad (19.7)$$

in which N_{core} is the effective (slab) index in the waveguide region (see Sec. 2.5.1) of Chapter 2 and k_0 is the wave number in vacuum. By substituting $\beta_0 \approx N_{\text{core}} k_0 - \frac{1}{2} \frac{k_{y0}^2}{N_{\text{core}} k_0}$ we find:

$$\Delta\beta_{0m} = \beta_0 - \beta_m = \frac{1}{2} m(m+2) \frac{k_{y0}^2}{N_{\text{core}} k_0} = \frac{m(m+2)}{3} \Delta\beta_{01} \quad (19.8)$$

in which

$$\Delta\beta_{01} = \frac{3\pi}{2N_{\text{core}} k_0 W^2}. \quad (19.9)$$

The length L_π over which the fundamental and the first order mode get π phase difference is related to $\Delta\beta_{01}$ according to:

$$L_\pi = \frac{\pi}{\beta_0 - \beta_1} \quad (19.10)$$

At length L the phase Φ_m of the modes is

$$\Phi_m = \beta_m L \quad (19.11)$$

and their phase difference $\Delta\Phi_{0m}$ with the fundamental mode is

$$\Delta\Phi_{0m}(L) = (\beta_0 - \beta_m)L = \frac{m(m+2)}{3} \pi \frac{L}{L_\pi} \quad (19.12)$$

Although the propagation constants that determine L_π can be approximated with equation 19.7 and effective index N_{core} , a much more accurate value for L_π is obtained when using a 2D mode solver on the actual MMI cross-section to determine β_0 and β_1 and then use equation 19.10 to calculate L_π . Alternatively, instead of the mode propagation constants, one can use the mode effective indices of the fundamental and first order modes, N_0 and N_1 obtained from the mode-solver, and use this equivalent relation to calculate L_π :

$$L_\pi = \frac{\lambda_0}{2(N_0 - N_1)}, \quad (19.13)$$

with λ_0 the vacuum wavelength.

a		m	0	1	2	3	4	5	6	7	8	9	...
b	General	$m(m+2)$	0	3	8	15	24	35	48	63	80	99	...
c	Symmetric	$m(m+2) \div 8$	0	-	1	-	3	-	6	-	10	-	...
d	Paired	$m(m+2) \div 3$	0	1	-	5	8	-	16	21	-	33	...
e	$L_{\text{si}} = 6L_\pi$	$\Delta\Phi_{0m,\text{si}} \bmod 2\pi$	0	0	0	0	0	0	0	0	0	0	...
f	$L_{\text{mi}} = 3L_\pi$	$\Delta\Phi_{0m,\text{mi}} \bmod 2\pi$	0	π	0	π	0	π	0	π	0	π	...
g	$L_{\text{3dB}} = \frac{3}{2}L_\pi$	$\Delta\Phi_{0m,\text{3dB}} \bmod 2\pi$	0	$\frac{3\pi}{2}$	0	$\frac{3\pi}{2}$	0	$\frac{3\pi}{2}$	0	$\frac{3\pi}{2}$	0	$\frac{3\pi}{2}$...

Table 19.1: The relative phase of the modes in an MMI-coupler for different lengths of the MMI-section and different excitation conditions.

19.3.1 Full image

From equation 19.12 we see that for a length $L = 6L_\pi$ the phase difference between the modes follows from

$$\Delta\Phi_{0m}(6L_\pi) = (\beta_0 - \beta_m) \cdot 6L_\pi = m(m+2) \cdot 2\pi \quad (19.14)$$

Table 19.1 row (b) shows the values of $m(m+2)$ for the different modes. For the self-imaging length

$$L_{\text{si}} = 6L_\pi \quad (19.15)$$

all modes have zero relative phase, apart from a multiple of 2π , as shown in Table 19.1, row (e), so that they will reproduce an image of the input field, as depicted in figure 19.4.

19.3.2 Mirrored Image

At half the self-imaging length $L = 3L_\pi$ the relative phase difference $\Delta\Phi_i = m(m+2) \cdot \pi$. We see that for even modes $m(m+2)$ is even, so $\Delta\Phi_{0m}$ will be zero, apart from a multiple of 2π , so all even modes have the same phase. For odd modes $m(m+2)$ is odd, so $\Delta\Phi_{0m}$ will equal π , apart from a multiple of 2π , as shown in row (f) of Table 19.1. If we separate the input field in an even and an odd part:

$$U(y, 0) = U_{\text{even}}(y, 0) + U_{\text{odd}}(y, 0) \quad (19.16)$$

we find

$$\begin{aligned} U(y, L) &= U_{\text{even}}(y, 0)e^{j\Delta\Phi_{\text{even}}} + U_{\text{odd}}(y, 0)e^{j\Delta\Phi_{\text{odd}}} \\ &= U_{\text{even}}(y, 0) - U_{\text{odd}}(y, 0) = U_{\text{even}}(-y, 0) + U_{\text{odd}}(-y, 0) \\ &= U(-y, L) \end{aligned} \quad (19.17)$$

So we see that at a length

$$L_{\text{mi}} = \frac{1}{2}L_{\text{si}} = 3L_\pi \quad (19.18)$$

mirrored image a mirrored image occurs, as shown in figure 19.4. Obviously a coupler with length L_{si} acts as a coupler in the bar state, whilst a coupler with length L_{mi} works as a cross coupler. By comparing with classical directional couplers (see Chapter 2, equation 2.96) we

Problem 19.1: Output signals of a 3-dB MMI-coupler.

Problem: Show that in a 2×2 MMI-coupler with length $\frac{3}{2}L_\pi$ the input signal at one port is equally divided over the two output ports, but with 90° phase difference.

Solution: By remembering that $U_{\text{odd}}(-y, 0) = -U_{\text{odd}}(y, 0)$ and $\frac{1}{2}\sqrt{2}(e^{-j\pi/4} + e^{j\pi/4}) = 1$, we find:

$$\begin{aligned}
 U(y, \frac{3}{2}L_\pi) &= U_{\text{even}}(y, 0) + U_{\text{odd}}(y, 0)e^{j3\pi/2} \\
 &= \frac{1}{2}\sqrt{2} \left(e^{-j\pi/4} + e^{j\pi/4} \right) \left\{ U_{\text{even}}(y, 0) + U_{\text{odd}}(y, 0)e^{j3\pi/2} \right\} \\
 &= \frac{1}{2}\sqrt{2} \left\{ \left(e^{-j\pi/4} + e^{j\pi/4} \right) U_{\text{even}}(y, 0) - \left(e^{j\pi/4} - e^{-j\pi/4} \right) U_{\text{odd}}(y, 0) \right\} \\
 &= \frac{1}{2}\sqrt{2} \left\{ e^{-j\pi/4} [U_{\text{even}}(y, 0) + U_{\text{odd}}(y, 0)] \right. \\
 &\quad \left. + e^{j\pi/4} [U_{\text{even}}(-y, 0) + U_{\text{odd}}(-y, 0)] \right\} \\
 &= \frac{1}{2}\sqrt{2}e^{-j\pi/4} \left\{ U(y, 0) + e^{j\pi/2} U(-y, 0) \right\} \\
 &= \frac{1}{2}\sqrt{2}e^{-j\pi/4} \left\{ U(y, 0) + jU(-y, 0) \right\}.
 \end{aligned}$$

If we discard the common phase term in the even and odd part we find:

$$U(y, \frac{3}{2}L_\pi) = \frac{1}{2}\sqrt{2} \left\{ U(y, 0) + jU(-y, 0) \right\}.$$

see that $L_{\text{mi}} = 3L_c$, in which $L_c = \pi/\Delta\beta_{01}$ is the length of a classical cross coupler. Now it looks as if the classical directional cross-coupler is shorter. This is not true, however, because in an MMI-coupler $\Delta\beta_{01}$ is significantly larger than in evanescently coupled waveguides.

19.3.3 3-dB coupler

Also MMI-couplers with a length $\frac{3}{2}L_\pi$ have interesting properties. From table 19.1 row (g) we see that the even modes have zero phase difference and the odd modes $\frac{3\pi}{2}$. So for the field $U(y, L = \frac{3}{2}L_\pi)$ we find after some manipulation (see problem 19.1):

$$U(y, \frac{3}{2}L_\pi) = \frac{1}{2}\sqrt{2} [U(y, 0) + jU(-y, 0)] \quad (19.19)$$

From this formula we see that at a length $\frac{3}{2}L_\pi$ the signal power is equally distributed over the direct image $U(y, 0)$ and the mirrored image $U(-y, 0)$, and that there is 90° phase difference between the two. So an MMI-coupler with a length $\frac{3}{2}L_\pi$ acts as a 3-dB hybrid coupler.

3-dB hybrid coupler

19.3.4 Restricted interference: symmetric excitation

Figure 19.5 shows the interference pattern in an MMI-section which is excited in the center by a (symmetric) single-mode waveguide. We see that with such an interference pattern a 1×2 coupler has half the length of a 1×1 coupler, a 1×3 coupler has $1/3$ of the length, a 1×4 coupler $1/4$, and so on.

Table 19.2: Summary of MMI-characteristics

Interference mechanism	General	Symmetric	Paired
Inputs \times Outputs	$N \times N$	$1 \times N$	$2 \times N$
First full image	$3L_\pi$	$3L_\pi/4$	L_π
First N -fold image	$3L_\pi/N$	$3L_\pi/4N$	L_π/N
Excitation requirements	none	$a_m = 0$ for $m = 1, 3, 5, \dots$	$a_m = 0$ for $m = 2, 5, 8, \dots$
Input locations	any	$y = 0$	$y = \pm W_e/6$

Symmetrically excited $1 \times N$ couplers can be much shorter than general MMI-couplers, because the odd modes are not excited and the interference pattern is formed only by even modes. The interference mechanism in such a coupler is called *restricted interference*, since not all modes participate in the imaging process. In table 19.1 row (b) we see that for all even modes $m(m+2)$ is a multiple of 8. This means that we get full imaging already at a length

$$L_{\text{si,symm}} = 6L_\pi/8 \quad (19.20)$$

and the length of a symmetric $1 \times N$ -coupler is shortened to

$$L_{1 \times N, \text{symm}} = 6L_\pi/8N \quad (19.21)$$

as shown in row (g) of table 19.1.

19.3.5 Restricted interference: paired interference

An interesting case occurs when we excite the MMI-section with waveguides positioned at $1/3$ and $2/3$ of the MMI-section width (i.e. at $y = \pm \frac{1}{6}W$). From figure 19.6 we see that if the excitation is symmetric around the dashed lines the modes $2, 5, 8, \dots$ will not be excited because they are anti-symmetric around these lines. So the interference pattern will be formed by modes 0 and 1 , 3 and 4 , 6 and 7 , and so on. That's why this case is called *paired interference*.

From row (d) in Table 19.1 we see that for these paired modes $m(m+2)$ is a multiple of 3, so a paired-interference coupler can be designed three times shorter than the general self-imaging coupler:

$$L_{\text{si,pi}} = L_{\text{si}}/3 \quad (19.22)$$

Because the modes penetrate slightly into the waveguide cladding layers (see Chapter 2, page 2-22), we have to use the effective width W_e rather than the physical width W of the MMI-section for an optimal design. Because the effective width differs for the different modes (it increases for higher order modes) full optimization of the input waveguide positions requires numerical simulations. In high-contrast waveguides the difference with positioning the waveguide at $y = \pm \frac{1}{6}W$ will be small.

Table 19.2 gives a summary of the different MMI-couplers discussed in this chapter. It is best to calculate L_π with a 2D mode solver and use equation 19.10 or 19.13. Use the proper entry from table 19.2 to calculate the length of the MMI.

19.4 MMI-couplers

19.4.1 Optimization of access waveguide width

Figure 19.7 shows simulated interference patterns in a 2×2 coupler for different access waveguide widths. For each case the same number of modes is used in the simulation of the MMI, but the excitation is different due to the difference in access waveguide width. Narrow access waveguides produce a large diffraction angle inside the MMI-section and, consequently, a small focal depth (see Chapter 2, equation 2.28). This is detrimental for the tolerance of the coupler. Small variations of the MMI-section width W lead to deviations of the modal propagation constants, which lead to a change in length $L_{3\text{dB}}$ at which the coupler forms its image. From the figure we see that for large waveguide widths, the divergence of the beam is small and, consequently, the depth over which the change in beam width is large, which makes the coupler less sensitive to fabrication tolerance. The trade-off is in device size. Although the multi-mode section is equally long for each case, the wider access waveguides typically require a taper to connect to a waveguide with standard width (see also figure 19.8, L_{tap}). This will increase the overall device size.

focal depth

fabrication tolerance

Figure 19.8 shows the schematic layout of an optimal design, including offsets at the junctions between access waveguides with different curvatures (see Chapter 10). This 2×2 MMI uses the paired interference mechanism. A detailed description is given by Hill [59]. From his study a ratio $\frac{w_a}{W} = 0.3$ appears to be a good design choice.

19.4.2 Design for low reflection

A disadvantage of deep-etched MMI-couplers is that they have significant reflections at the back-walls, as compared to directional couplers based on evanescent wave coupling. This can be particularly problematic in 1×2 MMIs that are operated in combiner mode where light enters at a waveguide on the two-waveguide side. There are a few design options for reducing these reflections.

reflection reduction

1. We can restrict the deep etched region to the side-walls of the MMI-section and apply a shallow etch at the back-walls of the MMI-coupler.
2. Instead of perpendicular back-walls we can angle the back-walls so that reflections are no longer directed to the input, as illustrated in Fig. 19.9. Because the light intensity beside the waveguide(s) at the back-wall is very low the effect of the angled back-wall on the transmission is very small. Figure 19.10 illustrates an advanced design, where side-walls and back-walls are only present where they are needed to define the waveguide edges, and are absent at positions where light does not interact with the walls. Figure 19.11 shows that an improvement of more than 20 dB is possible for a 1×2 combiner, with a proper choice of the angles as shown in Fig. 19.9. Experimental results show reflection reductions of 17.5 dB [279].

19.5 MMI mode filters

Multi-mode interference devices can be designed to act as a mode filter or a mode splitter. An example is given here of an MMI that is used as a mode-filter: it passes the

mode filter

mode splitter

Table 19.3: Design parameters of MMIs with unequal splitting ratio.

Split ratio	MMI length	Offset
$85 \div 15$	$\frac{3}{4}L_\pi$	$\pm W_{\text{MMI}}/4$
$72 \div 28$	$\frac{3}{5}L_\pi$	$\pm W_{\text{MMI}}/10$ and $\mp 3W_{\text{MMI}}/10$

fundamental mode but does not pass the first-order mode. The operation principle is illustrated with figure 19.12, that shows an MMI with a different geometry of input and output waveguides. The length of the MMI can be calculated with the use of table 19.2. We consider this MMI to be either a 1×1 MMI or a 4×4 MMI. The length of the 4×4 MMI (general interference) is $3L_\pi/N$, where $N = 4$ and that of the 1×1 MMI (symmetrical interference) is $3L_\pi/4N$, where $N = 1$. Both result in the same length, $L_{\text{MMI}} = \frac{3}{4}L_\pi$. So the same device can act differently, depending on the excitation. If we excite the MMI with a fundamental mode in the upper left waveguide (shown in red), the field will be split in 4 equal parts in the four outputs. If we excite the MMI with a fundamental mode in the (wider) central input (shown in blue), it will be imaged onto the central output. If we excite the MMI with the first-order mode in the central (wider) input (shown in green), this can be considered as exciting the MMI with a fundamental mode in both the 2nd and 3rd (narrow) input waveguides, with a 180° phase difference between them. This will result in each of them being split in 4 equal outputs, but with opposite phase in the center two output ports, thus canceling due to destructive interference, and with equal phase in the outer outputs, thus adding constructively.

A simulation of the operation of this device is illustrated in figure 19.13, which shows the intensity pattern of the light in the MMI mode-filter when it is excited with the fundamental mode (top figure) or when it is excited with the first order mode (bottom figure). The fundamental mode is imaged onto the output waveguide, whereas the first-order mode is imaged away from the output waveguide. Clearly, the facets of the MMI have to be angled to prevent reflections, as was explained in section 19.4.2.

angled facets

19.6 MMI with unequal splitting ratio

splitting ratio The MMI devices that have been discussed thus far all have equal splitting ratios: the $N \times N$ MMI splits a signal from one of the inputs N -ways, each with equal power. There are however two kinds of rectangular 2×2 MMIs that can be designed to split in unequal parts: $85 \div 15$ or $72 \div 28$. They are based on 4×4 and 5×5 MMIs, respectively, where the inputs are placed in such a way that images overlap in a partly constructive or partly destructive manner. The resulting devices have two input waveguides and two output waveguides and the higher splitting ratio is found in the cross port. Their design parameters are summarized in table 19.3 and illustrated schematically in figure 19.14. Further insight into the operation of such MMIs can be found in [280].

tapered MMI

Any arbitrary splitting ratio can be obtained by changing the shape of the MMIs. They are then no longer rectangular. By tapering the width of the MMI to be smaller or wider in the center of the device, any splitting ratio can be obtained. The working principle of these devices and guidance on their design can be found in [281].

19.7 MMI-reflectors

Another type of multi-mode interference device is the multi-mode interference reflector (MIR) [282, 63]. In its simplest form, it is based on a 1×2 MMI coupler, in which a reflector is placed at the end of the MMI. This results in the light being reflected back to the input waveguide. *MMI reflector*
MIR

Instead of a mirror reflector, two deep-etched back-walls at a 45° angle form a total-internal-reflection mirror (TIR mirror), as is shown in figure 19.15. This makes them easy to fabricate in a technology that supports deep-etched waveguides with reasonably vertical side walls. Due to the finite resolution of the fabrication process, the sharp corner of the tip of the reflector will be somewhat rounded. However, since the input field will focus halfway the 45° back-walls, there is no light at the rounded tip and the reflection will not be affected. *TIR mirror*

The MIR can be used as an alternative to other reflective elements, such as DBR mirrors, Sagnac loop mirrors or cleaved facets. In comparison, the MIR is small in size, has a broadband operation and can be placed anywhere on a chip, with lithographic precision.

MIR devices can be designed as 1-port reflectors, such as shown above, or 2-port reflectors, where 50% of the light is reflected back into the input waveguide and the other 50% reflects into a second port. Figure 19.16 shows a SEM-photograph of such a 2-port reflector. By adjusting the geometry, also reflectors with arbitrary splitting ratio can be designed. A detailed description is given in [63].

19.8 Mask design

Developing an MMI-device with optimized fabrication tolerance, reflection and transmission properties requires a major research effort. Generic foundries offer Process Design Kits (PDKs) in which a number of optimized designs are available to the user. *Process Design Kit*
PDK

These PDKs are tailored to the foundry process of the company that offers the PDK. Foundries may offer more than one PDK, for example with building blocks that cover different wavelength ranges. In this way, optimized MMI couplers could be available for use in the O-band, C-band or L-band.

In this section we give a brief explanation of an MMI-module that is available in a PDK for the C-band TU Eindhoven monolithic InP process. The use of the TU Eindhoven PDK is very similar to that of the other foundry PDKs. The examples below use the Nazca Design framework, but other design software would implement the similar mechanisms.

To design for a specific foundry, you must first review the foundry design manual. This document provides the user's perspective on the foundry process, outlining the available building blocks, the allocated design space and the design rules you must follow.

Some of the design rules, such as the minimum bending radius for curved waveguides, are automatically checked by your design software. Other rules, like the minimum lateral spacing of optical amplifiers, may not be flagged by the software. These are checked by the foundry during their design review process. Compliance with some of the rules is mandatory: failure to adhere to those rules will result in your circuit being rejected for fabrication. Other rules indicate that, although your circuit can be fabricated without technical problems, the resulting circuit may not work as expected. This could be the case for a curved waveguide with a very small bending radius.

The design example presented below is showing only a small fragment of a full design with a single building block, but it should give the reader a feeling for the processes involved.

19.8.1 1×2 MMI design

To design a 1×2 MMI for a particular foundry process, one typically has to load the foundry PDK and possibly other modules. In this case we load the Nazca Design framework itself (line 1 below) as well as the TU Eindhoven PDK for the generic InP fabrication process (line 2). The code would look like this:

```

1 import nazca as nd # Nazca Design framework
2 import tue_generic as tue # TU Eindhoven PDK
3
4 tue.WgShallow.strt(50).put()
5 tue.mm1x2_sh().put()
6
7 nd.export_gds()
```

Running the code results in a GDS file with structures as shown in figure 19.17a: a straight waveguide of $50 \mu\text{m}$ length, as specified in line 4 of the Nazca code, connected to a 1×2 MMI building block, as in line 5 of the code. The GDS file that was generated is what is needed for the foundry to fabricate the design.

However, for the actual device fabrication, some of the mask layers that are visualized in figure 19.17a are not relevant. They are just to give visual feedback to the user. In addition, they hide the actual building block implementation from the user. Such components are called *black-box* components or PCells and they may take parameters. An example of a parameterized building block would be an optical amplifier, where the length would be user-specified.

In order to make the lithographic masks needed to fabricate the device, the layers that are not present in the black-box representation should be added to the design GDS file. This is normally done by the foundry. They replace each black-box component with the actual layers that define that component. This is then called the *white-box* component. The example in figure 19.17b shows the layers that actually define the building block. In this particular example, the layers have the following meaning: the blue layer defines the waveguide; the pink layer the parts that should be (shallow) etched; the gray layer indicates where the etching should be deep. These different waveguide types have been previously described in section 1.4 and shown in figure 1.10.

The layers shown in figure 19.17b are not yet the final layers that define the photolithographic mask. In this example two physical masks are needed: one to define the shallow etch and one to define where the etching has to be deep. They are constructed from the layers shown in the figure by mask operations. The shallow etch is created by subtracting the (blue) waveguide layer from the (pink) etch layer. This results in the pattern shown in figure 19.18a. The pattern for the deep etch does not need further processing.

Careful observation of the white-box MMI, figure 19.17b, shows that the MMI is not defined by a simple rectangular structure. Rather it implements the angled facet as is presented schematically in figure 1.15.

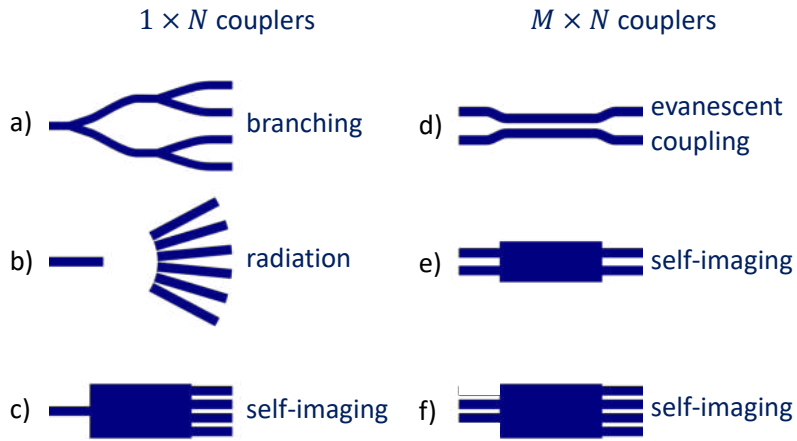


Figure 19.1: Different coupler types.

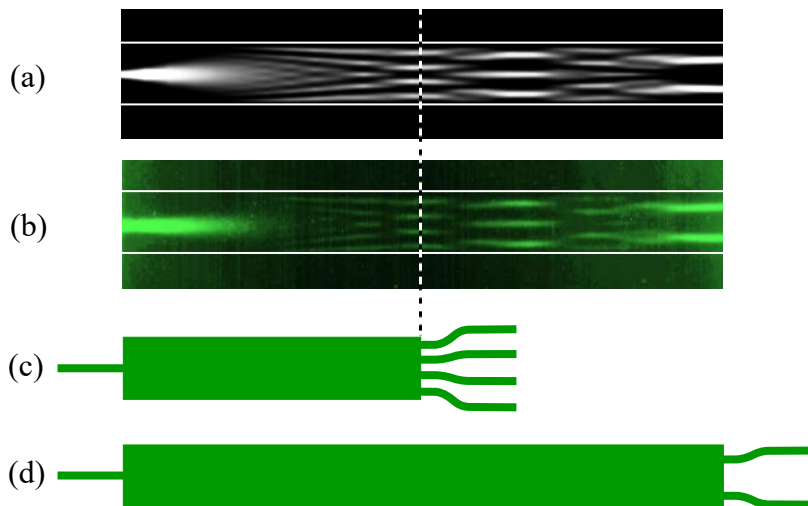


Figure 19.2: Multimode Interference
 a) simulated intensity pattern
 b) experimentally imaged pattern.
 c) layout of a 1×4 coupler
 d) layout of a 1×2 coupler

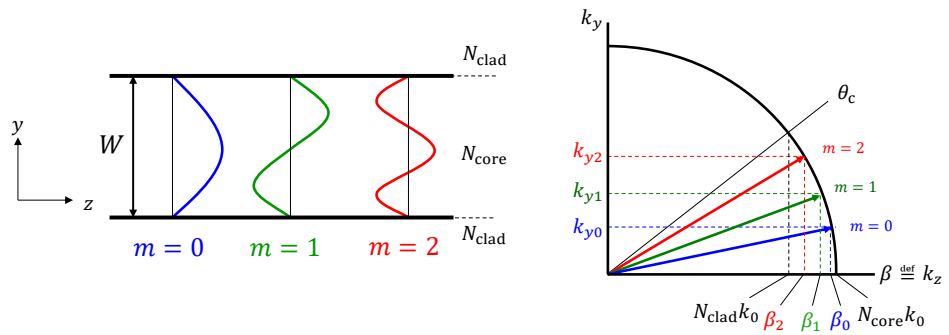


Figure 19.3: The relation between the lateral and the longitudinal propagation constants in a strongly multi-moded waveguide.

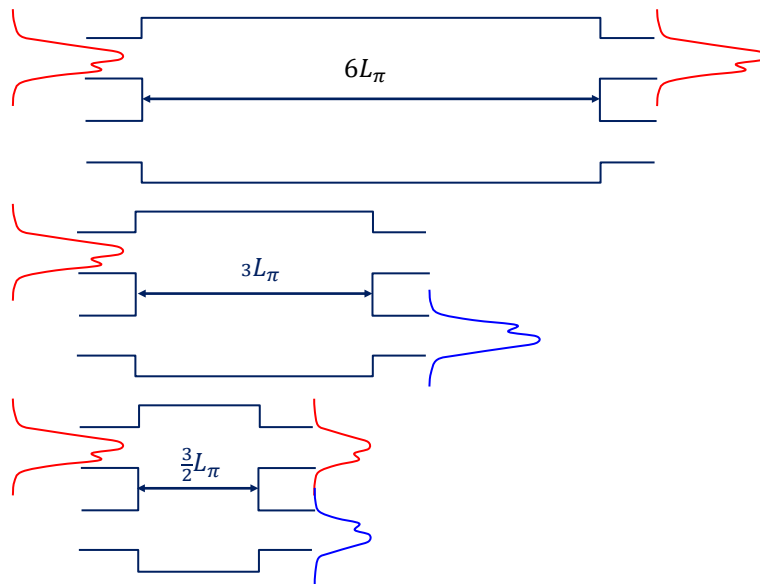


Figure 19.4: Self-imaging: bar coupler, cross coupler and 3-dB coupler.

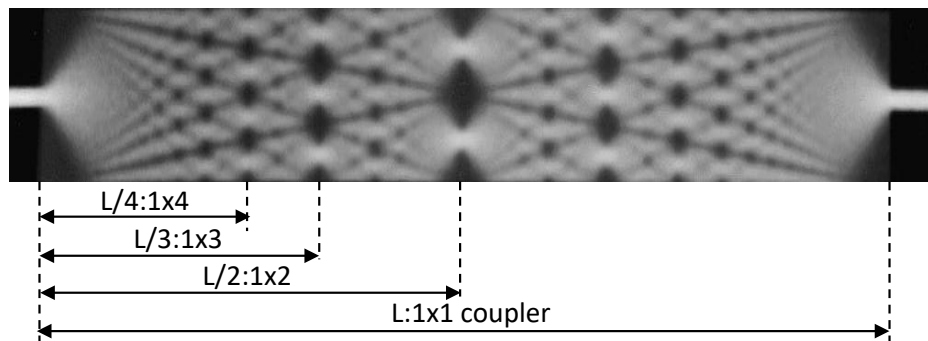


Figure 19.5: Interference pattern in a symmetrically excited coupler

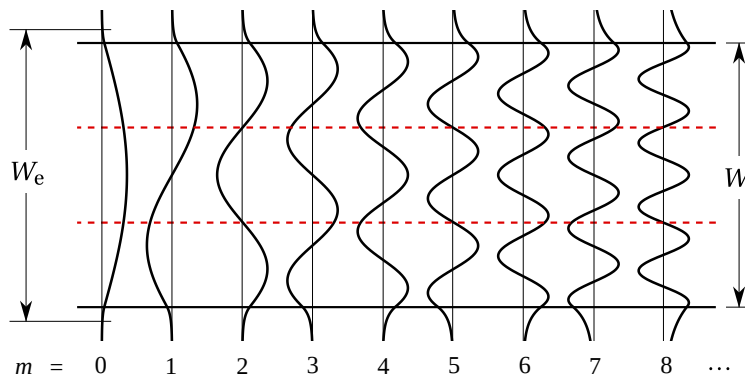


Figure 19.6: Interference pattern in a symmetrically excited coupler

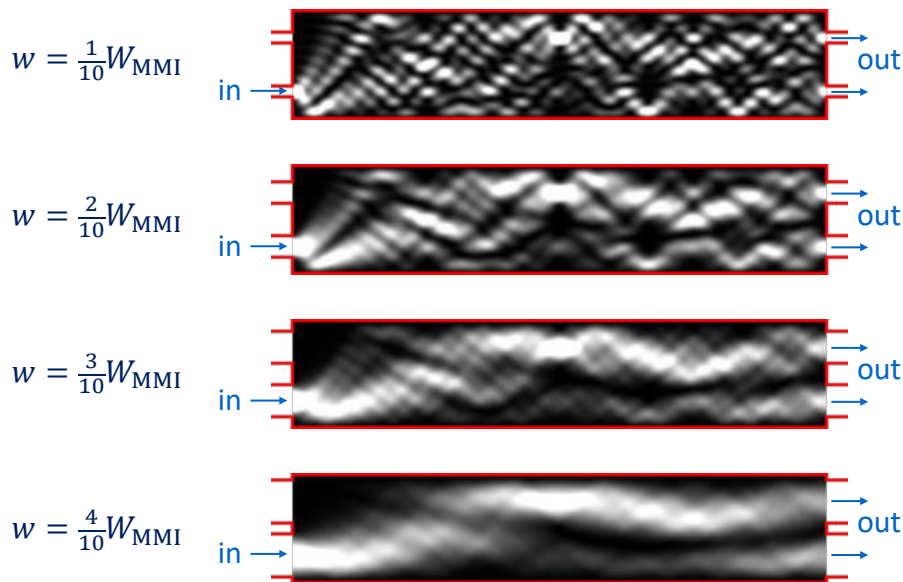


Figure 19.7: MMI intensity patterns for different access waveguide widths.

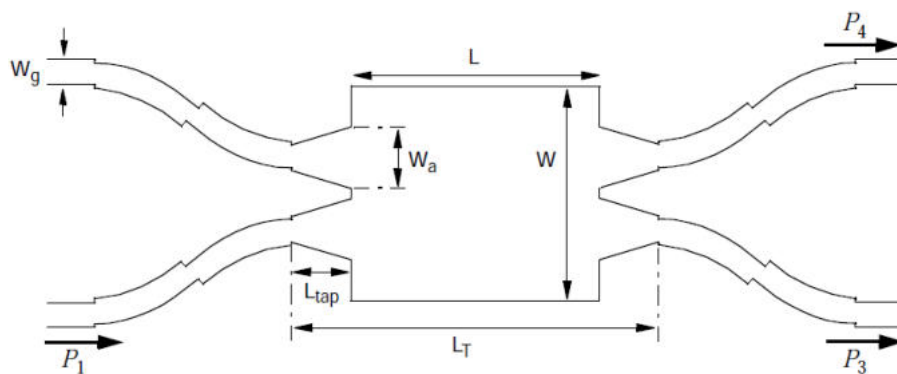


Figure 19.8: MMI intensity patterns for different access waveguide widths.

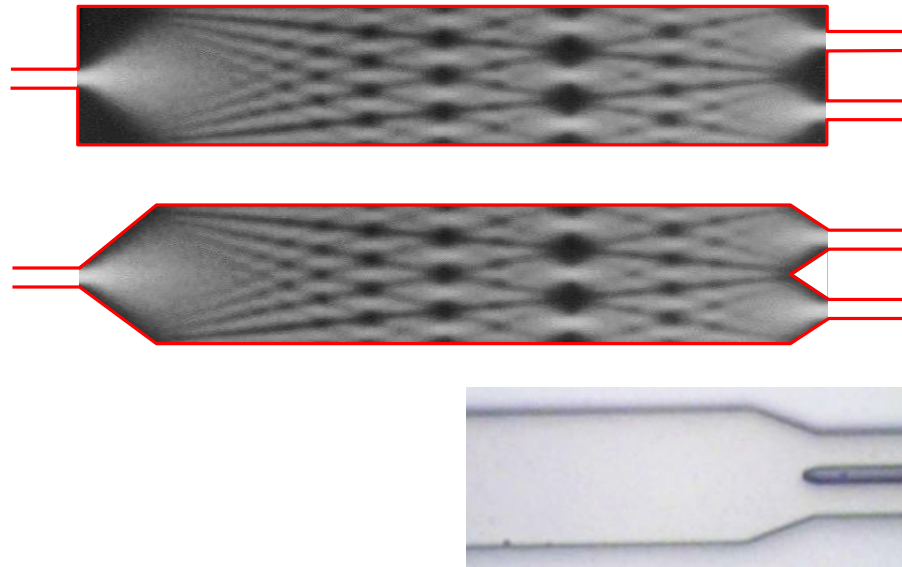


Figure 19.9: MMI-coupler with angled facets for reducing back reflections: simulations and microscope photograph [60].

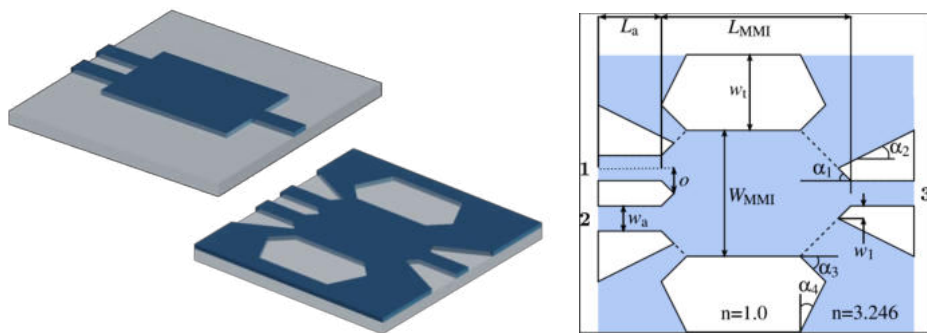


Figure 19.10: Optimized design for low reflection [279].

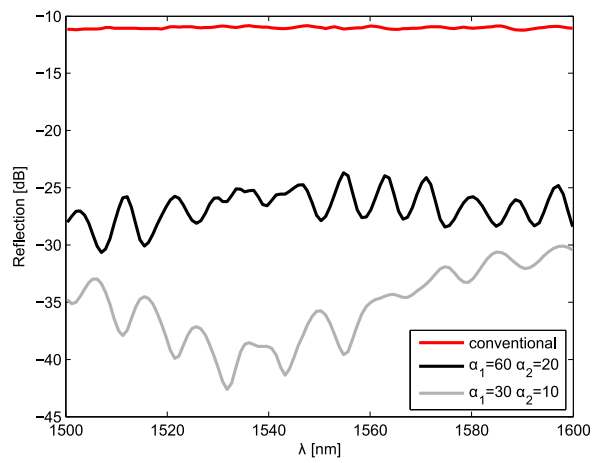


Figure 19.11: Reflection reduction for different facet angles [279].

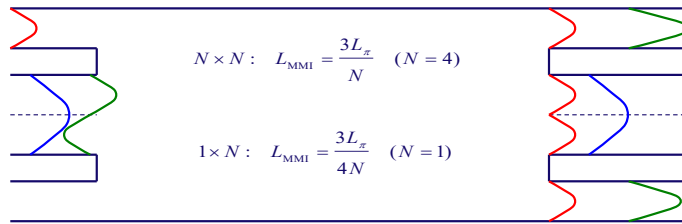


Figure 19.12: Schematic of mode-filter constructed from a 4×4 and 1×1 MMI.

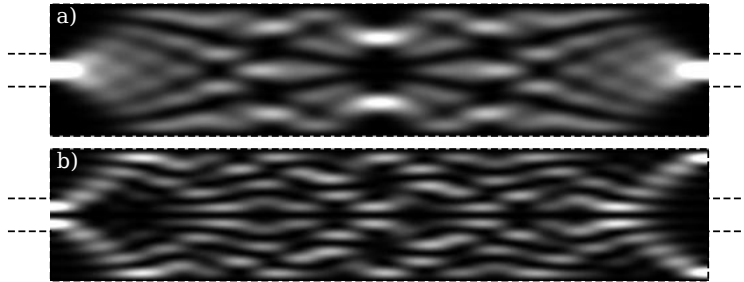


Figure 19.13: Simulated intensity pattern in MMI mode-filter, with a) fundamental mode excitation and b) first order mode excitation in the left input waveguide.

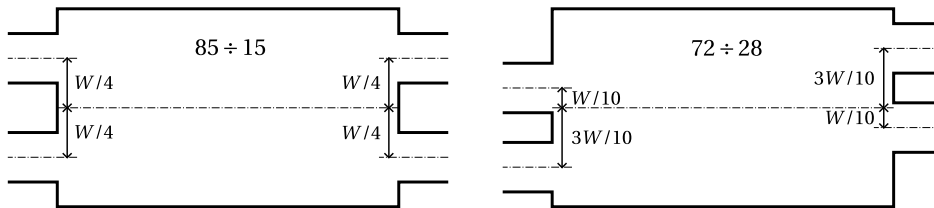


Figure 19.14: Geometry of the $85 \div 15$ and $72 \div 28$ MMIs. The higher ratio is found in the cross port.



Figure 19.15: Modal propagation simulation of a 1×2 MMI (top) and the corresponding 1-port multi-mode interference reflector (bottom).

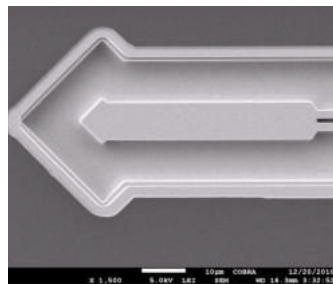


Figure 19.16: SEM Photograph of a 2-port MMI-reflector.

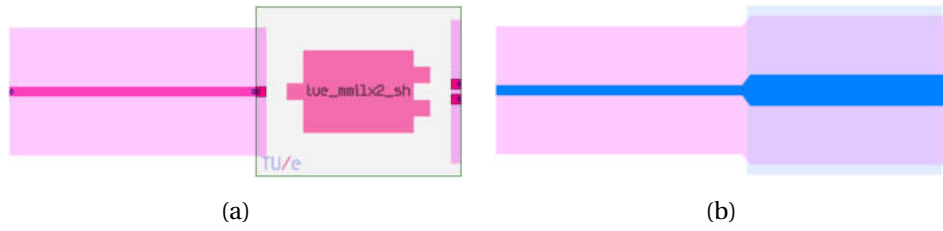


Figure 19.17: GDS file with (a) black-box and (b) white-box representations of the 1×2 MMI.

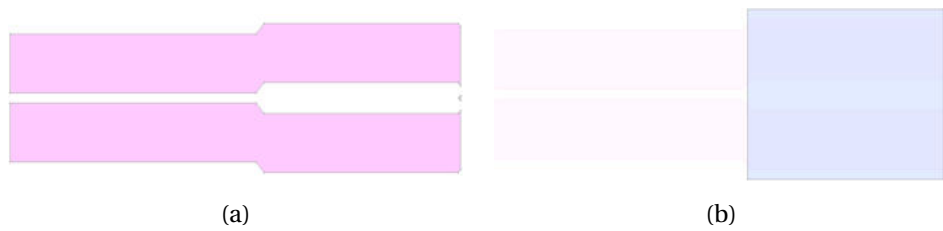


Figure 19.18: GDS file with (a) only the shallow-etch mask and (b) the deep-etch mask. For clarity, a faint view of the shallow-etch mask is visible with the deep-etch mask.